

Magnetic anisotropy of single-crystalline Mn₃Sn in triangular and helix-phase states

T. F. Duan, W. J. Ren, W. L. Liu, S. J. Li, W. Liu, and Z. D. Zhang

Citation: [Applied Physics Letters](#) **107**, 082403 (2015); doi: 10.1063/1.4929447

View online: <http://dx.doi.org/10.1063/1.4929447>

View Table of Contents: <http://scitation.aip.org/content/aip/journal/apl/107/8?ver=pdfcov>

Published by the [AIP Publishing](#)

Articles you may be interested in

[Structural and magnetic characterization of the intermartensitic phase transition in NiMnSn Heusler alloy ribbons](#)

J. Appl. Phys. **113**, 17A948 (2013); 10.1063/1.4800836

[Magnetic anisotropy energy of antiferromagnetic L1₀-type equiatomic Mn alloys](#)

Appl. Phys. Lett. **89**, 052504 (2006); 10.1063/1.2236103

[Multiple magnetic transitions and magnetoresistance anomalies in the Er_{0.9}Tb_{0.1}Mn₆Sn₆ compound](#)

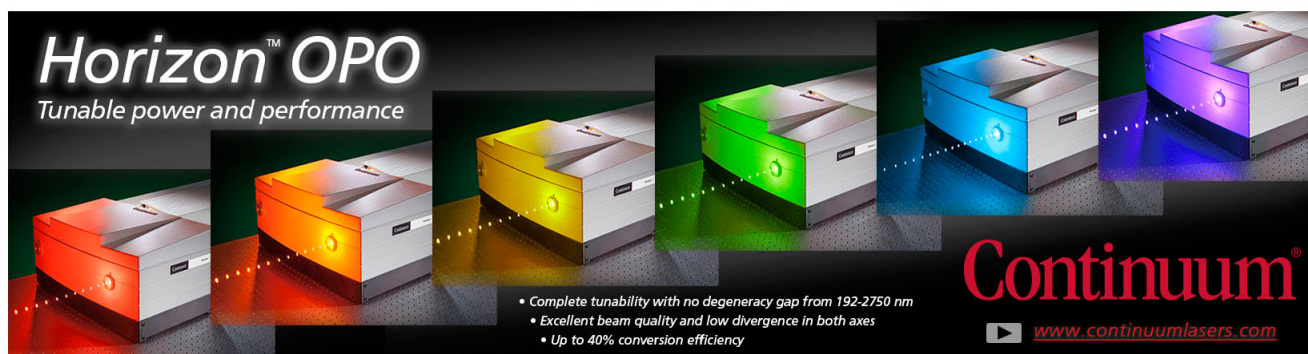
J. Appl. Phys. **93**, 6984 (2003); 10.1063/1.1556164

[Magnetic phase transitions in the system La_{1-x}Bi_xMnO_{3+λ}](#)

Low Temp. Phys. **28**, 569 (2002); 10.1063/1.1496669

[Magnetic properties of single-crystalline Mott insulator YVO₃](#)

J. Appl. Phys. **85**, 4850 (1999); 10.1063/1.370042

The advertisement features a row of five Continuum Horizon OPO laser units, each emitting a different color of light: red, orange, yellow, green, and blue. The text 'Horizon™ OPO' is prominently displayed in the top left, with the tagline 'Tunable power and performance' below it. In the bottom right, the Continuum logo is shown in red, with the website 'www.continuumlasers.com' and a play button icon. A list of features is provided in the bottom center: 'Complete tunability with no degeneracy gap from 192-2750 nm', 'Excellent beam quality and low divergence in both axes', and 'Up to 40% conversion efficiency'.



Magnetic anisotropy of single-crystalline Mn₃Sn in triangular and helix-phase states

T. F. Duan, W. J. Ren,^{a)} W. L. Liu, S. J. Li, W. Liu, and Z. D. Zhang

Shenyang National Laboratory for Materials Science, Institute of Metal Research, Chinese Academy of Sciences, Shenyang 110016, People's Republic of China

(Received 27 May 2015; accepted 10 August 2015; published online 24 August 2015)

The magnetic structure and phase transitions in single-crystalline Mn₃Sn with the D0₁₉ structure have been investigated by torque measurements and magnetic measurements. The results show that a triangular antiferromagnet (AFM) and a weak ferromagnet coexist above 270 K. At these temperatures, the torque measurements indicate a six-fold symmetry and another two-fold symmetry of the magnetic anisotropy. The [11 $\bar{2}$ 0] direction is the lowest-energy state in the triangular configuration. At low temperatures, two AFM helix-phase states are found in an applied magnetic field (H): In one of them, the [11 $\bar{2}$ 0] direction is the easiest deviation direction from the AFM state. In the other, it is the [0001] direction. The variation of the two states with temperature (T) and magnetic field is presented in an H - T phase diagram. © 2015 AIP Publishing LLC.

[<http://dx.doi.org/10.1063/1.4929447>]

Magnetism in systems with noncollinear magnetic structures is a subject of great interest due to the existence of a number of intriguing phenomena, such as spin frustration and topological phases,^{1,2} which show potential applied aspects in spintronic devices.³ Besides the triangular magnetic configuration in γ -Fe film⁴ and the spiral magnetic configuration in MnSi,⁵ (Fe,Co)Si,⁶ etc., the compound Mn₃Sn has attracted much attention since it presents either a triangular or a spiral magnetic configuration in different temperature ranges.⁷

As shown in Figs. 1(a) and 1(b), Mn₃Sn has the hexagonal Ni₃Sn-type (D0₁₉) of structure with space group $P6_3/mmc$ stacking sequence ABABAB.⁸ Mn₃Sn is an antiferromagnet (AFM) with a Néel temperature (T_N) of 420 K. The magnetic configuration is triangular at 300 K, as demonstrated by powder neutron diffraction. Another magnetic transition occurs at $T_1 = 270$ K.⁹ Nagamiya *et al.*^{10,11} have proposed two models for the spin orders: below T_1 , the spin configuration is spiral, and above T_1 , it is triangular. T_1 is very sensitive to composition and heat treatment.^{12,13} Feng *et al.*¹⁴ have studied the magnetic order of Mn₃Sn at low temperatures on a polycrystalline sample and found glassy ferromagnetism below (T_f) = 31.8 K. Tomiyoshi *et al.*^{15–21} have performed detailed neutron diffraction on a Mn₃Sn single crystal and have concluded that the compound is dominantly AFM with weak ferromagnetism (WFM) between T_1 and T_N . The triangular antiferromagnetic configuration is caused by the Dzyaloshinskii-Moriya (D-M) interaction, and the WFM originates from the distortion of the equilateral triangle and the non-stoichiometry of the compound that a few Sn atoms are replaced by Mn atoms. Cable *et al.*^{7,22–24} performed neutron diffraction on a single crystal and found that, below T_1 , the period of the helix structure is 11c (22 layers). Neutron diffraction has revealed that only the inverse-triangular-structure spin configuration explains the WFM.²⁵ Zhang *et al.*²⁶ and Sandratskii and Kübler^{27,28} have

calculated the spin configuration of Mn₃Sn by first-principles density-functional theory and spin-density-functional theory, respectively. The triangular spin configuration was found to be most stable. Sandratskii and Kübler²⁷ found that, in this spin configuration, the spin direction parallel to [11 $\bar{2}$ 0] is the lowest-energy state when the spin-orbit coupling (SOC) is switched on. However, this lowest-energy state has not been confirmed by experiments yet. In the present paper, six-fold symmetry in the (0001) plane is reported for this triangular configuration and the lowest-energy direction of the triangular spin configuration is confirmed. Below 270 K, two helix-phase states have been identified by magnetization and torque measurements on the Mn₃Sn single crystal.

At first, polycrystalline Mn₃Sn weighted 30 g was produced by melting together stoichiometric amounts of the constituent metals, with purity higher than 99.9%, in an arc furnace under a high-purity argon atmosphere. Single-crystalline Mn₃Sn was prepared by melting the polycrystalline material at 1273 K in an alumina crucible sealed in a quartz tube filled with a small amount of high purity argon. The crucible was slowly cooled to 873 K at a rate of 2 K/h. According to Tomiyoshi,¹⁶ Mn₃Sn is stable only in the presence of excess Mn, that is, Sn atoms at 2c sites of the space group $P6_3/mmc$ are partially substituted by Mn atoms. Therefore, there must be excess Sn in the ingot, and when the crystal was grown, the excess Sn would be distributed among crystals, which is benefit to separate the crystals. Many single crystals are obtained by crushing the crucible and a 5.5 mg approximately hexagonal-sharped crystal was selected by good sharp to study the properties of the compound. Structural characterization was performed by means of Cu- K_α x-ray diffraction (XRD), scanning electron microscopy (SEM, XL30, PHILIPS), and electron probe microanalysis (EPMA, 1610, SHIMADZU). Quantitative EPMA analysis showed that the composition of the single crystal is Mn_{3.13}Sn. However, for simplicity, the composition of the crystal will be written as Mn₃Sn in the present paper. The XRD patterns of Mn₃Sn single crystals with (0001) and

^{a)}Electronic mail: wjren@imr.ac.cn

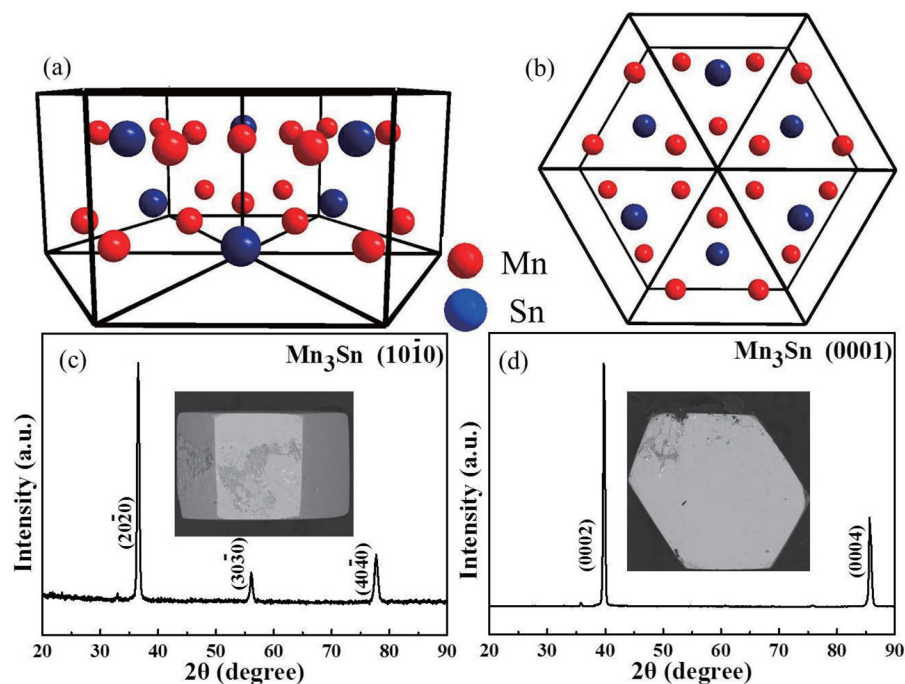


FIG. 1. Crystal structure and XRD patterns of a Mn_3Sn single crystal. (a) and (c) $(10\bar{1}0)$ -plane model and XRD pattern, respectively; (b) and (d) (0001) -plane model and XRD pattern, respectively. The insets in (c) and (d) are SEM images of the single crystal examined with XRD.

$(10\bar{1}0)$ surface planes are shown in Figs. 1(c) and 1(d), and the weak reflections at 33.0° (near the $(20\bar{2}0)$ reflection) in Fig. 1(c) and 35.7° (near the (0002) reflection) and 75.8° (near the (0004) reflection) in Fig. 1(d) are $\text{Cu-}K_\beta$ reflections that have remained after filtering. The crystal has the hexagonal Ni_3Sn -type of structure with $a=0.5671$ nm and $c=0.4536$ nm. The insets in Figs. 1(c) and 1(d) show the SEM images of the hexagonal (0001) basal plane and the rectangular $(10\bar{1}0)$ lateral plane.

The magnetic properties were investigated by means of a Physical Property Measurement System (PPMS, Quantum Design). Vibrating-sample-magnetometer (VSM), torque-magnetometer, and heat-capacity options of the PPMS were used to study the physical properties of the Mn_3Sn single

crystal. The magnetization was measured as a function of temperature in the temperature range from 330 to 150 K and the susceptibility from 200 to 300 K. The specific heat was measured under the condition of a 1% temperature pulse with the temperature-pulse method. The magnetic-torque was measured in the temperature window from 200 to 300 K at a magnetic field of 50 kOe. The magnetization of the Mn_3Sn single crystal was measured as a function of temperature at a magnetic field of 200 Oe applied along different directions. As can be seen in Fig. 2(a), for both the $[0001]$ and $[11\bar{2}0]$ directions, the magnetization exhibits a steep increase at 270 K, the increase for the $[11\bar{2}0]$ direction being more than five times larger than for the $[0001]$ direction. Below 270 K, the difference of the increasing magnetization

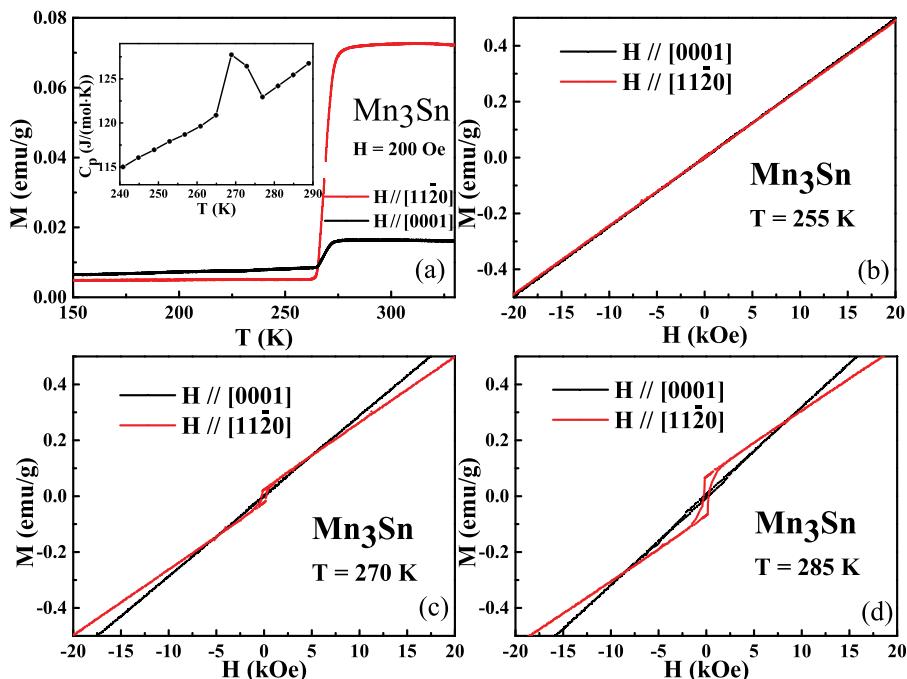


FIG. 2. (a) Temperature dependence of the magnetization of Mn_3Sn in a magnetic field of 200 Oe and (b)–(d) hysteresis loops measured at 255 K, 270 K, and 285 K, respectively. The inset in (a) shows the heat capacity of Mn_3Sn .

between the $[0001]$ and $[11\bar{2}0]$ directions decreases. The heat capacity, shown in the inset of Fig. 2(a), presents an anomaly at around 270 K, which indicates a phase transition. Figures 2(b), 2(c), and 2(d) show the magnetization vs field curves at 255 K, 270 K, and 285 K, respectively. With increasing temperature, the magnetization measured with the field in the $[11\bar{2}0]$ direction changes from a linear dependence on the field to magnetic-hysteresis behavior, whereas the magnetization remains almost linear for the field in the $[0001]$ direction. For the $[11\bar{2}0]$ direction, the magnetic phase transition from helix AFM to triangular AFM with WFM occurs, as has been reported by Cable *et al.*²⁴ and Brown *et al.*²⁵ based on neutron-diffraction experiments. The WFM may arise from a distortion of the equilateral triangular spin configuration.¹⁵

Figure 3(a) shows torque measurements in the temperature window from 260 to 280 K in a field of 50 kOe applied parallel to the (0001) plane. Below 270 K, the torque τ changes only little with θ , with indication of a period of 180° . This may be associated with the helix spin configuration that has been established by Cable *et al.*^{7,22} via neutron diffraction. Above 270 K, the curves exhibit clear structure. The curve at 280 K, also shown in Fig. 3(b), has been selected for further analysis as an example. Above 270 K, the torque approximately has a period of 180° shown by dashed dotted line with another period of 60° shown by the dashed line superimposed on it. The period of 180° probably arises from distortion of the equilateral triangular spin configuration and the period of 60° from the magnetocrystalline anisotropy in the $(10\bar{1}0)$ plane. Thus, the expression

$$\tau = K_2 \sin 2\theta + K_6 \sin 6\theta \quad (1)$$

may be suitable for fitting the torque curve. In Eq. (1), τ is torque, θ is the angle between the initial position and the position when the sample has rotated anticlockwise, K_2 is the anisotropy constant associated with the distortion of the equilateral triangular spin configuration, and K_6 is defined as the magnetocrystalline anisotropy constant contributed by the triangular spin configuration Mn atoms. The solid line is the fitting curve with $K_2 = 2760$ ergs/cm³ and $K_6 = -2210$ ergs/cm³, which has satisfactory accuracy. By the way, the definition of the angle θ is different from the conventional definition that is the angle between magnetization direction and the easy axis, so an easy direction occurs at zero torque, positive slope. Therefore, in our fitting, $E_{an} = 0$ is a dividing line. When $E_{an} > 0$, the position at $E_{an} = 0$ is the easy direction; when $E_{an} < 0$, the position at $E_{an} = 0$ is the hard direction. Because $K_6 < 0$ and $H \parallel [10\bar{1}0]$ direction at $\theta = 0^\circ$, the half-periodic position ($\theta = 30^\circ$), which is the $[11\bar{2}0]$ direction, is the easy magnetization direction for the triangular spin configuration of the Mn atoms. The conclusion is in agreement with Sandratskii and Kübler in Ref. 27 (situation in Fig. 1(c)). Because the integral of τ over θ represents the anisotropy energy of magnetic materials, the anisotropy energy should have a period of 180° shown by the solid line in Fig. 3(c), which is constituted of a six-fold symmetric anisotropy shown by dashed-dotted line superimposed on another two-fold symmetric anisotropy shown by dotted line in Fig. 3(c). Although the anisotropy-energy values corresponding to the fitting line are

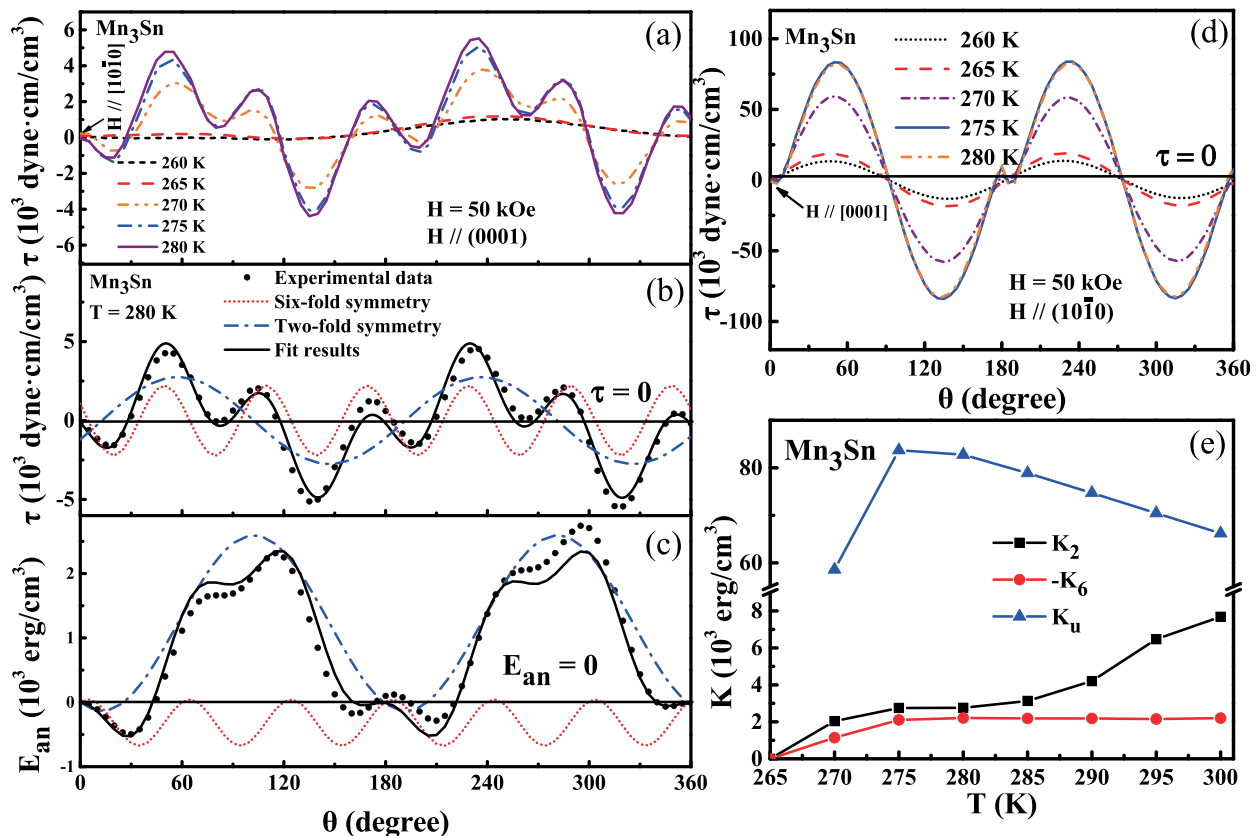


FIG. 3. Torque at a magnetic field of 50 kOe in the temperature range from 260 to 280 K for (a) the (0001) plane and (b) the $(10\bar{1}0)$ plane. (c) Fit of the torque for the (0001) plane at 280 K. (d) Temperature dependence of the anisotropy constants of Mn_3Sn at 50 kOe.

not precisely the same as the experimental data, they have the same period. So, the little differences may originate from the shape anisotropy which is small compared with the other anisotropy-energy contributions. The theoretical analysis of the Mn_3Sn triangular-configuration energy in the (0001) plane in Refs. 9, 10, and 14 gives the $\sin 6\theta$ term that arises from the D-M interaction and the exchange interaction in the (10 $\bar{1}$ 0) plane. The $\sin 2\theta$ term comes from the magnetic interlayer interaction. Sandratskii and Kübler^{27,28} have added SOC to calculate the total energy of Mn_3Sn and suggest that the SOC plays an important role in the weak ferromagnet Mn_3Sn . The spin parallel to the $[11\bar{2}0]$ direction is the lowest-energy state. So, the torque measurement gives experimental support for the theory of Sandratskii and Kübler.

In the initial situation in the torque measurement, H is parallel to the [0001] direction in the (10 $\bar{1}$ 0) plane, as shown in Fig. 3(d). Below 270 K, the curves are well represented by a sinusoidal function. Above 270 K, near 0° and 180° , the curves have another periodicity which indicates another lowest-energy position. So, in the (10 $\bar{1}$ 0) plane, there are two minimal-energy positions which are different from the [0001] direction.

By fitting the torque curves at the various temperatures, defining the maximum of the torque in the (10 $\bar{1}$ 0) plane as K_u , the anisotropy constants have been obtained as a function of temperature, as shown in Fig. 3(e). As can be seen, in the

stable triangle phase above 275 K, K_u with the magnitude of 10^4 ergs/cm³ decreases with increasing temperature, K_2 with the magnitude of 10^3 ergs/cm³ increases, and K_6 with the magnitude of 10^3 ergs/cm³ is nearly consistent.

In order to investigate the situation at lower temperatures, the torque and magnetization were also measured in the temperature range from 150 to 270 K, as shown in Fig. 4. In Fig. 4(a), the torque curves of the (10 $\bar{1}$ 0) plane at 50 kOe show a transition at 245 K, which indicates that the $[11\bar{2}0]$ direction is the lowest-energy direction in the plane below 245 K and the [0001] direction above 245 K. Figure 4(b) shows torque measurements with H parallel to the (0001) plane. The very small torque values present no substantial difference at all angles below 270 K which indicates that the structure does not change. The magnetization vs field curves along the $[11\bar{2}0]$ and the [0001] directions are shown in Figs. 4(c) and 4(d) at 225 K and 260 K, respectively. All four magnetization curves are linear but, at 225 K (below 245 K), the $[11\bar{2}0]$ direction has the largest magnetization whereas, at 260 K (above 245 K), the [0001] direction has the largest magnetization. So, there are two AFM helix phase states in an applied magnetic field: In one state, the [0001] direction is an easier magnetization direction than the $[11\bar{2}0]$ direction. In the other state, the situation is opposite. As can be seen in Fig. 4(e), the temperature dependence of the magnetization in the two different directions shows the same crossover at

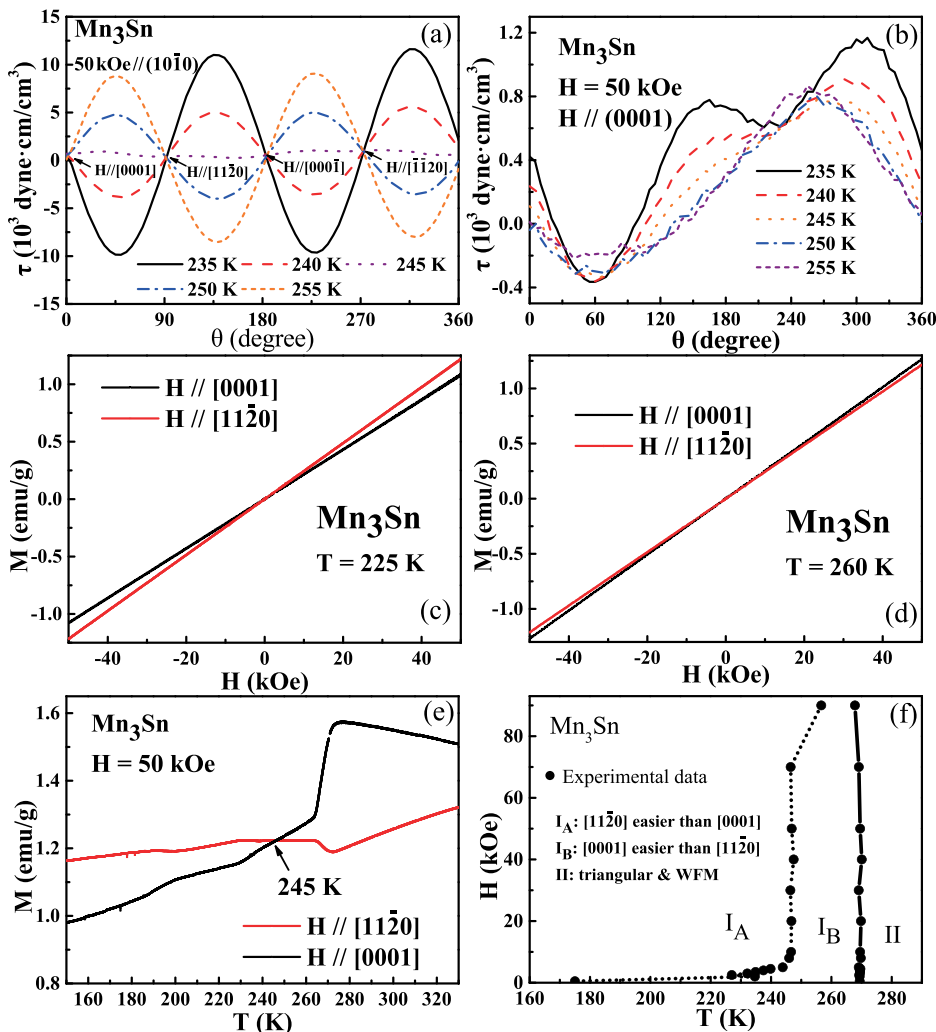


FIG. 4. Torque at a magnetic field of 50 kOe in the temperature range from 235 to 255 K for (a) the (10 $\bar{1}$ 0) plane and (b) the (0001) plane. (c) Temperature dependence of the magnetization at 50 kOe. (d) Magnetic phase diagram of Mn_3Sn in the temperature interval from 150 to 290 K. In area I_A , the $[11\bar{2}0]$ direction is an easier magnetization direction than the [0001] direction. In area I_B , the [0001] direction is an easier than $[11\bar{2}0]$. In area II, triangular AFM and WFM coexist.

245 K as the torque experiment. Therefore, by measuring the field dependence of the magnetization along the two different directions and determining the temperature of equal magnetization (T_2) in the two directions, we can construct the magnetic phase diagram in Fig. 4(f). The T_2 and T_1 lines divide the H - T plane into three regions. In area I_A , the $[11\bar{2}0]$ direction is the easy deviation direction from AFM, whereas, area I_B , it is the $[001]$ direction. In the phase diagram, we see that, below 245 K, the I_A - I_B transition from the $[11\bar{2}0]$ direction to the $[0001]$ direction is very sensitive to temperature and applied field. In area II, triangular AFM and WFM coexist.

In conclusion, by torque measurements, six-fold and two-fold symmetries in the (0001) plane have been established, associated with the magnetocrystalline anisotropy and distortion of the equilateral triangular spin configuration, respectively. It has also been demonstrated that the $[11\bar{2}0]$ direction is the lowest-energy state in the triangular spin configuration. The conclusions obtained from the magnetization and torque measurements are summarized in a magnetic phase diagram.

This work has been supported by the National Basic Research Program of China (Grant No. 2012CB619404) and the National Natural Science Foundation of China (Grant No. 51331006).

- ¹S. H. Kang, S. Shan, A. Kosmrlj, W. L. Noorduin, S. Shian, J. C. Weaver, D. R. Clarke, and K. Bertoldi, "Complex ordered patterns in mechanical instability induced geometrically frustrated triangular cellular structures," *Phys. Rev. Lett.* **112**, 098701 (2014).
- ²F. Jonietz, S. Muhlbauer, C. Pfleiderer, A. Neubauer, W. Munzer, A. Bauer, T. Adams, R. Georgii, P. Boni, R. A. Duine, K. Everschor, M. Garst, and A. Rosch, "Spin transfer torques in MnSi at ultralow current densities," *Science* **330**, 1648–1651 (2010).
- ³I. Žutić, J. Fabian, and S. Das Sarma, "Spintronics: Fundamentals and applications," *Rev. Mod. Phys.* **76**, 323–410 (2004).
- ⁴R. Ritz, M. Halder, M. Wagner, C. Franz, A. Bauer, and C. Pfleiderer, "Formation of a topological non-Fermi liquid in MnSi," *Nature* **497**, 231–234 (2013).
- ⁵P. Milde, D. Kohler, J. Seidel, L. M. Eng, A. Bauer, A. Chacon, J. Kindervater, S. Muhlbauer, C. Pfleiderer, S. Buhbrandt, C. Schutte, and A. Rosch, "Unwinding of a skyrmion lattice by magnetic monopoles," *Science* **340**, 1076–1080 (2013).
- ⁶E. Lhotel, V. Simonet, J. Ortloff, B. Canals, C. Paulsen, E. Suard, T. Hansen, D. J. Price, P. T. Wood, A. K. Powell, and R. Ballou, "Domain-wall spin dynamics in kagome antiferromagnets," *Phys. Rev. Lett.* **107**, 257205 (2011).

- ⁷J. W. Cable, N. Wakabayashi, and P. Radhakrishna, "A neutron study of the magnetic-structure of Mn_3Sn ," *Solid State Commun.* **88**, 161–166 (1993).
- ⁸J. T. Kandra, J. Y. Lee, and D. P. Pope, "Deformation of single-crystal Mn_3Sn ," *Mater. Sci. Eng., A* **145**, 189–198 (1991).
- ⁹J. S. Kouvel, "Exchange anisotropy and long-range magnetic order in the mixed intermetallic compounds, $(MnFe)_3Sn$," *J. Appl. Phys.* **36**, 980–981 (1965).
- ¹⁰T. Nagamiya, S. Tomiyoshi, and Y. Yamaguchi, "Triangular spin configuration and weak ferromagnetism of Mn_3Sn and Mn_3Ge ," *Solid State Commun.* **42**, 385–388 (1982).
- ¹¹T. Nagamiya, "Triangular spin ordering in Mn_3Sn and Mn_3Ge ," *J. Phys. Soc. Jpn.* **46**, 787–792 (1979).
- ¹²G. Zimmer and E. Kren, "Investigation of the magnetic phase transformation in $MnSn$," *AIP Conf. Proc.* **5**, 513 (1972).
- ¹³E. Kren, J. Paitz, G. Zimmer, and E. Zsoldos, "Study of magnetic phase-transformation in Mn_3Sn phase," *Physica B+C* **80**, 226–230 (1975).
- ¹⁴W. J. Feng, D. Li, W. J. Ren, Y. B. Li, W. F. Li, J. Li, Y. Q. Zhang, and Z. D. Zhang, "Glassy ferromagnetism in Ni_3Sn -type $Mn_{3,1}Sn_{0,9}$," *Phys. Rev. B* **73**, 205105 (2006).
- ¹⁵S. Tomiyoshi and Y. Yamaguchi, "Magnetic-structure and weak ferromagnetism of Mn_3Sn studied by polarized neutron-diffraction," *J. Phys. Soc. Jpn.* **51**, 2478–2486 (1982).
- ¹⁶S. Tomiyoshi, "Polarized neutron-diffraction study of the spin structure of Mn_3Sn ," *J. Phys. Soc. Jpn.* **51**, 803–810 (1982).
- ¹⁷S. Tomiyoshi, S. Abe, Y. Yamaguchi, H. Yamauchi, and H. Yamamoto, "Triangular spin structure and weak ferromagnetism of Mn_3Sn at low-temperature," *J. Magn. Magn. Mater.* **54**, 1001–1002 (1986).
- ¹⁸H. Ohmori, S. Tomiyoshi, H. Yamauchi, and H. Yamamoto, "Spin structure and weak ferromagnetism of Mn_3Sn ," *J. Magn. Magn. Mater.* **70**, 249–251 (1987).
- ¹⁹S. Tomiyoshi, H. Yoshida, H. Ohmori, T. Kaneko, and H. Yamamoto, "Electrical-properties of the intermetallic compound Mn_3Sn ," *J. Magn. Magn. Mater.* **70**, 247–248 (1987).
- ²⁰P. Radhakrishna and S. Tomiyoshi, "A neutron-scattering study of the magnetic excitations in a triangular itinerant antiferromagnet, Mn_3Sn ," *J. Phys.: Condens. Matter* **3**, 2523–2527 (1991).
- ²¹S. Tomiyoshi, Y. Yamaguchi, and Y. Ito, "A Mn_3Sn neutron polarizer," *Physica B* **213**, 932–934 (1995).
- ²²P. Radhakrishna and J. W. Cable, "Magnetic excitations in the triangular antiferromagnet Mn_3Sn ," *J. Magn. Magn. Mater.* **104**, 1065–1066 (1992).
- ²³J. W. Cable, N. Wakabayashi, and P. Radhakrishna, "Magnetic excitations in the triangular antiferromagnets Mn_3Sn and Mn_3Ge ," *Phys. Rev. B* **48**, 6159–6166 (1993).
- ²⁴J. W. Cable, N. Wakabayashi, and P. Radhakrishna, "Structure of the modulated magnetic phase of Mn_3Sn ," *J. Appl. Phys.* **75**, 6601 (1994).
- ²⁵P. J. Brown, V. Nunez, F. Tasset, J. B. Forsyth, and P. Radhakrishna, "Determination of the magnetic-structure of Mn_3Sn using generalized neutron polarization analysis," *J. Phys.: Condens. Matter* **2**, 9409–9422 (1990).
- ²⁶D. L. Zhang, B. H. Yan, S. C. Wu, J. Kübler, G. Kreiner, S. S. P. Parkin, and C. Felser, "First-principles study of the structural stability of cubic, tetragonal and hexagonal phases in Mn_3Z ($Z = Ga, Sn$ and Ge) Heusler compounds," *J. Phys.: Condens. Matter* **25**, 206006 (2013).
- ²⁷L. M. Sandratskii and J. Kübler, "Role of orbital polarization in weak ferromagnetism," *Phys. Rev. Lett.* **76**, 4963–4966 (1996).
- ²⁸L. M. Sandratskii, "Noncollinear magnetism in itinerant-electron systems: Theory and applications," *Adv. Phys.* **47**, 91–160 (1998).